



Published as: *Integr Biol (Camb)*. 2009 June ; 1(5-6): 371–381.

## Systemic *in vivo* distribution of activatable cell penetrating peptides is superior to cell penetrating peptides

Todd A. Aguilera<sup>1,2</sup>, Margaret M. Timmers<sup>1</sup>, Emilia S. Olson<sup>1,2</sup>, Tao Jiang<sup>1,3</sup>, and Roger Y. Tsien<sup>1,3</sup>

<sup>1</sup>Department of Pharmacology, University of California at San Diego, La Jolla, CA 92093-0647

<sup>2</sup>Department of Medical Scientist Training Program, University of California at San Diego, La Jolla, CA 92093-0647

<sup>3</sup>Department of Howard Hughes Medical Institute, and University of California at San Diego, La Jolla, CA 92093-0647

### Abstract

Cell penetrating peptides (CPPs) have been developed as vehicles for payload delivery into cells in culture and in animals. However several biologic features limit their usefulness in living animals. Activatable cell penetrating peptides (ACPPs) are polycationic CPPs whose adsorption and cellular uptake is minimized by a covalently attached polyanionic inhibitory domain. Cleavage of the linker connecting the polyanionic and polycationic domains by specific proteases (tumor associated matrix metalloproteases discussed herein) dissociates the polyanion and enables the cleaved ACPP to enter cells. In contrast to CPP counterpart, ACPPs are relatively nonadherent and distributed uniformly to normal tissues. While nonaarginine (r<sub>9</sub>) CPP administered intravenously into mice initially bind to the local vasculature and redistribute to the liver, where > 90% of the injected dose accumulates 30 min after injection. Regardless of the presence of the polyanionic inhibitory domain, confocal imaging of live tissues reveals that the majority of the ACPP and CPP remain in punctate organelles, presumably endosomes. Therefore further improvements in the efficiency of delivery to the cytosol and nucleus are necessary. In addition to improved target specificity, a major advantage of ACPPs over CPPs for potential clinical applications is reduced toxicity. Systemically administered r<sub>9</sub> CPP causes acute toxicity in mice at a dose 4 fold lower than the MMP cleavable ACPP, a complication not observed with an uncleavable ACPP presumably because the polycationic charge remains masked systemically. These data suggest that ACPPs have greater potential than CPPs for systemic delivery of imaging and therapeutic agents.

### Introduction

Polycationic cell penetrating peptides (CPPs), also known as protein transduction domains (PTDs), have been proposed for many years as vehicles for intracellular delivery of payloads from small polar molecules to large macromolecules and nanoparticles.<sup>1,2</sup> Most published successes have been on model membranes or cells in culture, though clinically relevant delivery of drugs or contrast agents will require *in vivo* efficacy. Early reports that systemic administration could give efficient intracellular delivery need re-examination because cell uptake was assessed after fixation, which is now known to enable entry into cells.<sup>3,4,5</sup> In most efficacious *in vivo* applications of CPPs, the peptides were locally injected into tumors<sup>6,7</sup> or into the peritoneum to deliver to intraperitoneal (ip) tumors.<sup>8,9</sup>

In this report we describe *in vivo* pharmacokinetic and toxicity problems of CPPs and show that many of them can be ameliorated by conversion to activatable CPPs (ACPPs). ACPPs consist of a polycationic CPP (typically arg<sub>9</sub> or r<sub>9</sub>) connected via a cleavable linker to a matching polyanion (typically glu<sub>9</sub> or e<sub>9</sub>), which reduces the net charge to nearly zero and thereby inhibits adhesion and uptake into cells. Lower case letters indicate D-amino acids, which are preferred within the polyanion and polycation to minimize proteolysis. Upon cleavage of the linker, the polyanion is released, locally unmasking the polyarginine and its inherent adhesiveness (Fig. 1A).<sup>10</sup> This mechanism implies that the affinity of the polyglutamate for the polyarginine is strong enough for efficient intramolecular hairpin formation, yet weak enough to dissociate after linker cleavage. Before discussing the pharmacokinetics and toxicity in animals, we discuss validation of multiple components of the ACPP design. We now show by isothermal calorimetry that the dissociation constant of e<sub>9</sub> for r<sub>9</sub> is in the appropriate range for effective masking of the CPP to be switched on upon cleavage. We also verify the *in vitro* selectivity of our workhorse matrix metalloprotease (MMP) linker, PLGLAG, for cleavage by a wide range of enzymes. Unlike 2-D cultures, 3-D cultures accumulate enough endogenous extracellular proteases to trigger ACPP cleavage and uptake, yet 3-D cultures are still thin and transparent enough to validate protease triggered ACPP accumulation and determine subcellular localization. The question of *in vivo* selectivity is addressed in the companion paper (Olson et al).

The simple r<sub>9</sub> CPP initially binds to the vasculature at the site of injection then redistributes mainly to the liver, as previously seen with systemic administration of Tat peptide from HIV. 11.<sup>12</sup> ACPPs access tissues more broadly, have longer circulation, are excreted by both renal and hepatobiliary routes, are less toxic, and enable targeting to tumors expressing enzymes that cleave the linker. Another controversial issue regarding CPPs is whether they can efficiently deliver cargoes to the cytoplasm and nucleus, not just endosomes or other punctate organelles. Most reports on verifiably live cells in standard two-dimensional tissue culture demonstrate that significant (> 10%) escape from endosomes requires at least several micromolar CPP depending upon the cell type and culture conditions.<sup>13</sup> Because our culture models rarely had cytosolic and nuclear uptake of CPP and ACPPs, we have taken an independent approach to determine subcellular localization in animals after systemic injection. We harvest live tissues and image them immediately with confocal microscopy. Live observation is important because after cell death the peptide redistributes to the nucleus in the same way that fixation and cell death is known to permit redistribution of CPPs. We find that at doses below systemic toxicity levels, almost all of the CPP payloads remain within punctate organelles in all tissues imaged. Therefore, improved mechanisms for endosomal escape will be needed to deliver payloads efficiently to the cytosol and nucleus in living animals.

## Results

### Determining the affinity of arg<sub>9</sub> for glu<sub>9</sub> *in vitro*

In order for the e<sub>9</sub> domain of an ACPP to block cell uptake of the r<sub>9</sub> CPP that could be restored following proteolysis, the r<sub>9</sub> must be intramolecularly complexed with the e<sub>9</sub> while the linker is intact, which means that the dissociation constant of a bimolecular e<sub>9</sub>-r<sub>9</sub> complex, K<sub>d</sub>, should be much less than the effective molarity (EM) imposed by the linker. A linker of 6 amino acid residues plus an 6-aminohexanoyl spacer consists of about 25 single bonds, which corresponds to an EM of 49 mM.<sup>14</sup> To test the aforementioned hypothesis that K<sub>d</sub> << EM for ACPP's, we compared this literature value for EM to an experimental value for K<sub>d</sub> determined by isothermal titration calorimetry (ITC). We synthesized model polyanionic (Suc-e<sub>8</sub>, where the succinyl group is glutamate without the N-terminal amine) and polycationic (r<sub>9</sub>) peptides, both amidated at their C-termini. We measured their mutual affinity by ITC at physiological ionic strength and temperature. The advantage of ITC is that it requires neither spectroscopic labels nor

attachment to a solid support, either of which might perturb the affinity. Multiple ITC runs with Suc-e<sub>8</sub> titrated into r<sub>9</sub> or vice versa at different concentrations and corrected for heats of dilution, gave a K<sub>d</sub> of (6 ± 0.7) μM (mean ± s.d.), well below EM = 49 mM as required for essentially complete formation of an intramolecular hairpin. Fig. 1B and C show a representative uncorrected experiment and the corresponding corrected titration curve fit which yielded a K<sub>d</sub> in this case of 5.9 μM.

After protease cleavage of the linker, the free concentrations of the e<sub>9</sub> and r<sub>9</sub> must be below the K<sub>d</sub> in order for them to substantially dissociate and allow cell uptake of the r<sub>9</sub>. Typical doses of ACPPs for optical imaging are 10 nmol per 25 g mouse or 0.4 μmol/kg. Even if all the ACPP were fully cleaved but none excreted, the total concentration of e<sub>9</sub> and r<sub>9</sub> would be submicromolar, and the free concentrations would be yet lower due to binding to membranes and macromolecules. Cleavage-dependent dissociation of e<sub>9</sub> from r<sub>9</sub> is robust because the intramolecular EM with an intact linker is orders of magnitude higher than the free concentration of each fragment after cleavage.

### Selectivity for MMP-2 and MMP-9 *in vitro*

To assess the enzyme selectivity of our initial MMP-cleavable ACPP, suc-e<sub>8</sub>-xPLGLAG-r<sub>9</sub>-c (Cy5) (x= aminohexanoic linker) was incubated for 30 minutes with 50 nM each of seven MMPs (1, 2, 3, 7, 8, 9 and 14) and seven other enzymes (neprilysin, cathepsin B, urokinase (uPa), tissue plasminogen activator (tPa), thrombin, prostate specific antigen (PSA), and plasmin. The resulting mixtures were then subjected to polyacrylamide gel electrophoresis, separating cleaved product from uncleaved starting material. MMP-2, 8, 9, and 14 all cleaved a significant amount of the peptide, with MMP-2 and -9 causing near complete cleavage after just 30 minutes (Fig. 1D). This data demonstrates that the PLGLAG substrate is preferentially cleaved by gelatinases MMP-2 and 9 over the other enzymes tested. Under similar conditions, MMP-2 and -9 did not attack a cleavage resistant control with D-amino acid linker xplglag (Fig. 1E).

### MMP-based ACPP's are selectively taken up tumor cell clusters in a 3D culture model

Even though cell lines such as HT-1080 secrete MMP-2 and -9, those enzymes become notably diluted in the supernatants of traditional 2-dimensional culture, causing slow ACPP cleavage and negligible uptake. Previously, we found that significant cleavage and uptake of ACPPs required precleavage with exogenous protease.<sup>10</sup> Nevertheless a higher-density culture system in which endogenously secreted proteases accumulate sufficiently to mediate localized cleavage and uptake of peptide would be quite useful. Compared to solid tumors *in vivo*, cultures have greater transparency, enable better subcellular resolution of peptide localization, allow for easy discrimination between live and dead cells, and circumvent systemic pharmacokinetics for early validation of imaging peptides. We therefore decided to test a three-dimensional culture model in which invasive cancer cells degrade the extracellular matrix, a process that has been shown to involve MMPs.<sup>15</sup>

We grew MDA-MB-231 human adenocarcinoma cells and HT-1080 human fibrosarcoma cells suspended in matrigel to assay ACPP uptake. Confocal maximum projections in Fig. 2A–D show Cy5 fluorescence (red) from MDA-MB-231 cell clusters treated with cleavable PLGLAG ACPP in the absence and presence of GM6001, a broad-spectrum MMP inhibitor. Also shown are clusters treated with a cleavage-resistant control with a D-amino acid linker (plglag), and a positive control CPP, r<sub>9</sub>-c(Cy5), that requires no cleavage. Cells were preloaded with calcein green AM (green fluorescence) to verify cell. The imaging demonstrated that the cleavable ACPP accumulated to levels nearly as high as that of the positive control CPP, and that uptake was significantly diminished upon addition of the MMP inhibitor or replacement of L-amino acids by D-amino acids. These data were quantified using Cy5 intensities averaged over regions

within 20 to 40 3D clusters of MDA-MB-231 and HT1080 cells imaged using a fluorescent dissecting microscope (Fig. 2E and example shown in Supp. Fig. 1). The overall dynamic range between the positive and negative controls was 4 to 10-fold. Upon close examination of the confocal images, cells that proved to be dead based upon counterstain always had nuclear colocalization of peptide whether CPP, ACP or cleavage resistant control. The peptide was determined using confocal microscopy to be either in subcellular punctae, on the surface of the cells, or in the adjacent extracellular matrix as a light cloud surrounding the 3D cluster as better visualized by confocal slice of ACP treatment (Fig. 2F).

### ACPPs have more tractable pharmacokinetics than CPPs

To evaluate biodistribution, 10 nmol either of CPP or full length ACP was injected into the tail vein of mice bearing HT-1080 tumors. Much of the fluorescence of the CPP was immediately retained in the vein near the site of injection and slowly washed out over the following 6 hrs (Fig. 3A). Fluorescence intensity in the blood decreased to near baseline within minutes after injection (Fig. 3B). Most tissues of mice injected with the CPP appeared dimly fluorescent 30 minutes after injection and continued to gradually lose fluorescence over the next few hours, suggesting immediate distribution from blood to tissues followed by gradual clearance (Fig. 3C).

In contrast, the ACP did not remain at the site of injection but rather diffused evenly throughout the tail and tissues (Fig. 3A). The circulation time was much greater for the ACP, whose blood levels took 30 minutes to decline to levels reached by the CPP after 3 minutes (Fig. 3B). Finally, after 30 minutes the ACP appeared more fully distributed throughout tissues suggesting that inhibition of the sticky polyarginine by the polyglutamate enabled much greater initial distribution throughout the mouse (Fig. 3C). After 6 hours, circulating ACP peptide was largely washed out of the animals. In ACP injected animals, greater fluorescence remained, which revealed tumor contrast. These observations suggest that the CPP had limited initial tissue distribution due to its adhesive nature, whereas the ACPs were able to more fully distribute into tissues allowing opportunity for enzyme cleavage to unmask the CPP and enable greater retention in target tissues.

In order to quantify the amount of uptake into different critical organs (tumor, muscle, liver, and kidney), we determined the standardized uptake value (SUV) (moles recovered/g tissue)/(moles injected/weight of animal). Tissue preparation and SUV computation are described in detail in the Experimental section. The measured SUVs for this series of HT1080-bearing nude mice are shown in Fig. 3D, which reveals a time dependent change and differential distribution between the cleavable ACP and CPP. The tumor SUV was slightly but not significantly greater for ACP than CPP at 30 minutes. Uncleaved and presumably some cleaved peptide washed out by 6 hours, resulting in lower SUVs for both peptides. The similarity of CPP and ACP SUVs measured in tumor homogenates was surprising given that the ACP consistently gave much higher fluorescence intensity in intact tumors. Possible reasons for this discrepancy are considered in the Discussion. Tumor uptake of ACP at 6 hours was roughly 4-fold greater than in muscle, the most significant adjacent tissue to tumor. Based on the measured SUV, 174 nmoles/kg or 1.7% ID/g was delivered to tumor from the 10 nmol injection. The liver retained the majority of CPP, presumably because CPP stuck to the liver during the first pass. In contrast the kidney retained the ACP, presumably due to its inability to adhere to cells until cleaved, resulting wider body distribution and later renal filtration.

To more clearly understand the pharmacokinetics, the % injected dose can be calculated from the measured SUVs in the liver and kidney, which revealed a significant difference between the CPP and ACP distribution 30 minutes after injection and at 6 hours. The average weight of the livers from these animals was 1190 mg and for the two kidneys was 333 mg. The measured SUVs using these tissue weights translated into a ten-fold difference (90% vs. 8%)

in CPP uptake after 30 minutes in liver and kidney respectively. After 6 hours, the uptake in these organs had changed minimally (84% vs. 9%). Adding the inhibitory  $e_9$  decreased liver uptake by a factor of 4.5 and increased kidney by more than a factor of 3 at the early time point (21% vs. 28%) and this difference was augmented at 6 hours (33% vs. 48%). Based on these data it became clear that nearly all of the sticky CPP accumulated rapidly in the liver, whereas much of the ACPP remained in circulation after 30 minutes where it was cleared mainly through the kidney and less by liver, as evidenced by different SUVs at 6 hours. Overall, these results reveal greater ability of ACPPs to reach most target tissues, where cleavage by disease-associated proteases can trigger accumulation, as shown in the accompanying paper (Olson *et al*) by directly comparing L-amino acid with cleavage resistant D-amino peptides.

### Confocal microscopy of living tissues reveals punctate subcellular distribution of CPPs and ACPPs

CPPs have been advocated for many years as potential vehicles for intracellular delivery beyond endosomes of bioactive macromolecules in animals. However, most attempts to demonstrate vehicle delivery have been done in tissue culture, and validation in animals is rarely attempted.<sup>1,2,16</sup> Since most bioactive cargoes would have to reach the cytosol or nucleus to be effective, we used confocal imaging to examine the subcellular distribution of fluorescence signal after IV injection of CPP and ACPP in HT1080 xenografted mice. Animals that were pre-injected with the ACPP and CPP were re-injected with intravenous Hoechst 33342 (to stain nuclei) and 5 MDa rhodamine dextran (to stain the blood pool) five minutes before sacrifice. At 30 minutes and 6 hours post peptide injection, tissues were removed, kept on ice in HBSS, and imaged using confocal microscopy. Tissues were imaged in the order of kidney, liver, tumor (when applicable) and muscle, mostly due to differing tolerances of live tissue to the effects of hypoxia. Fig. 4 shows confocal slices of the CPP and ACPP in muscle, liver, and kidney. Uptake in the muscle was notably low for both peptides with most of the peptide found in intracellular non-nuclear puncta that were in close proximity to blood vessels. Consistent with gross imaging and SUVs, the liver showed much higher fluorescence for CPP versus ACPP at both 30 minutes and 6 hours, though the localization was very similar. Confocal imaging revealed that neither peptide was significantly detectable in the nucleus. Instead, peptide was localized to subcellular puncta and possibly along the sinusoids adjacent to the vascular flow, although this was less clear. Excretion via the bile into the duodenum was detected as early as 30 minutes post injection as shown in Supp. Fig. 2.

The kidney had the reverse distribution as the liver, with the ACPP accumulating to a much higher degree than the CPP (Fig. 4C), consistent with SUV measurements (Fig. 3D). It was surprising that ACPPs in kidney appeared brighter at 30 minutes compared to 6 hours when the SUV suggested otherwise, an observation that held true for the CPP in the liver. We hypothesize that this difference (microscopy vs. homogenate) occurred because when high concentrations of peptide are present, self-quenching of the fluorescent tag is more likely to occur, thus affecting quantitative imaging. Self-quenching was observed in SUV homogenates at very high concentrations but was accounted for using SUV standard curves. Renal excretion of the ACPP was evidenced by fluorescence signal of the urine present in the bladder 30 minutes after injection (Supp. Fig. 2) but this was not quantified. The kidney uptake was predominantly in luminal puncta (white arrows) of the tubules, suggesting that the 2–5 kDa peptides were filtered and endocytosed in the renal tubules and completely excreted. Again there was no detectable peptide in the nuclei of kidney cells for either peptide (Fig. 4C). For each tissue a short time series was taken to confirm that the fluorescence contained in intracellular vesicles continued to move around inside the cells, suggesting that the cells were alive (data not shown). When the tissues sat on coverslips as dry mounts over time, the peptide shifted its distribution to the nuclei as shown in the kidney (Supp. Fig. 3), likely due to loss of membrane integrity

and/or cell death. These observations highlight the ease with which misassignment of peptide localization occurs unless properly controlled.

### Confocal microscopy reveals no obvious detectable nuclear uptake of ACPPs and CPPs in live tumor and stroma of xenografted mice

By thorough visual inspection of confocal stacks of various tissues including tumors, it became evident that neither ACPP nor CPP yielded detectable nuclear uptake in intact living cells, as discussed above (Fig. 4). Fluorescence signal was about four times higher for the ACPP than for the CPP (Fig. 5A and B), but was mostly in perinuclear puncta for both peptides. Nuclear uptake was below the detection limit as confirmed by scrolling through z sections of confocal stacks (Fig. 5A and B). Many nuclei, especially in the core of the tumor, failed to label with Hoechst 33342. Perhaps this small molecule is eliminated from the circulation before it reaches the poorly perfused interior of a xenograft. However, the cells at the tumor stroma/ capsule boundary that had highest level of peptide uptake had detectable Hoechst labeled nuclei. Because endosomal escape and nuclear uptake of CPPs in monolayer tissue culture often requires concentrations of several  $\mu\text{M}$  or more,<sup>16,17</sup> we injected one mouse with 100 nmol or 5  $\mu\text{mol/kg}$  of ACPP, 10 times the usual dose, but there was still no detectable nuclear uptake in any tissue (data not shown). Presumably the local concentration of free CPP stayed well below the threshold of several  $\mu\text{M}$  necessary for cytosol and nuclear uptake in culture, because lack of complete ACPP proteolysis and an excess of binding sites within compacted tissue *in vivo*. However final concentration determined for CPP in the liver and ACPP in the kidney was up to 8–17  $\mu\text{mol/kg}$  based on SUV assuming 20–25g mouse from just a 10 nmol injection (Fig. 3D). Further consideration of direct systemic injection of free CPPs at  $\geq 5 \mu\text{mol/kg}$  (100 nmol) was impractical due to systemic toxicity (see below). The tumor stroma/ capsule as shown in Fig. 5A and B was much brighter for the ACPP than for the CPP, as more clearly shown by fluorescence and hematoxylin/ eosin histology (Fig. 5C and D). This difference reflects protease dependent activation and uptake as analyzed further in the accompanying paper (Olson *et al*)

### ACPPs decrease acute toxicity of CPPs because of the linked polyanionic inhibitory domain

Although CPPs have been proposed for many years as vehicles for macromolecular drug delivery very little has been reported regarding their systemic toxicity. Because large quantities of peptides were required for such studies and to avoid toxicity from the fluorescent tag, three unlabeled peptides were synthesized with C-terminal amides: r<sub>9</sub> (CPP), Suc-e<sub>8</sub>-xPLGLAG-r<sub>9</sub> (cleavable ACPP), and Suc-e<sub>8</sub>-(PEG2)<sub>2</sub>-r<sub>9</sub> (uncleavable control, where PEG2 = -NH(CH<sub>2</sub>CH<sub>2</sub>O)<sub>2</sub>CH<sub>2</sub>CH<sub>2</sub>NHCOCH<sub>2</sub>CH<sub>2</sub>CO-). Acute toxicities are summarized in Table 1. At an intravenous dose of 100 nmol or 5  $\mu\text{mol/kg}$ , 10-fold higher than the imaging dose of 10 nmol, the CPP was acutely toxic. These animals appeared to go into shock with visibly dilated blood vessels and died of respiratory collapse within one minute after bolus injection. The anesthesia was then changed from injectable ketamine/ midazolam to isoflurane, a volatile anesthetic that is more rapidly reversible (30s to 1 min). Under these conditions and with reduction of the CPP dose to 2.5  $\mu\text{mol/kg}$ , 4 out of 5 mice survived the injection. Clinically however, they showed signs of respiratory distress, which was resolved as they recovered from anesthesia after about one minute. Subsequently the animals showed signs of visible vasodilation and were slightly sedated but responsive to stimulation for 10–20 minutes after injection. After this initial recovery period, the mice appeared perfectly normal and lost no significant weight over the following 24 hour period. When the injection was increased to 5  $\mu\text{mol/kg}$ , under the same anesthesia conditions, none of 5 mice survived the first few minutes. Death appeared to be due to immediate respiratory failure with mild vasodilation.

We hypothesized that the systemic toxicity of the CPP was associated with the large positive charge causing mast cell degranulation as previously discussed.<sup>18</sup> We tested our hypothesis

that the polyanionic motif of ACPP would inhibit this acute toxicity by injecting a starting dose of 5  $\mu\text{mol/kg}$ . Indeed, this dose appeared to have no acute effect. When the dose was increased to 10  $\mu\text{mol/kg}$  all five mice survived but troubling clinical signs began to appear, including vasodilation and sedation beginning two to three minutes after recovery from anesthesia. Animals slowly became unresponsive to toe pinch and remained in a sedated state for 30 minutes to 90 minutes, after which they recovered full alertness and behaved normally. The mice lost no more than 1 gram of weight over the first 24 hours and the surviving mice continued to thrive. The dose was then increased to 20  $\mu\text{mol/kg}$  and none of 5 mice survived longer than 15 minutes at this increased dose. Death appeared to be due to respiratory failure following cardiovascular collapse, as described earlier for CPP's but was delayed for ACPPs.

Although the maximum tolerated dose of the cleavable ACPP was about 4-fold higher than that of the CPP, the symptoms of toxicity were roughly similar though delayed, suggesting that the toxicity of the cleavable ACPP may be due to a fraction of molecules undergoing nonspecific proteolysis and release of their CPP components. If so, the control uncleavable peptide should have even less systemic toxicity. To test this hypothesis, two mice were initially injected with 10  $\mu\text{mol/kg}$  of the uncleavable control and both survived. The mice woke up within the first minute with normal behavior and no signs of vasodilation. At 20  $\mu\text{mol/kg}$  2/2 survived with no clinical signs of stress. Mice were then injected with 50  $\mu\text{mol/kg}$  and there was no sign of toxicity in 3/3 mice. This dose is 20 fold greater than the maximum tolerated dose of the CPP and indicates that the tandemly fused anionic segment reduces CPP toxicity by at least this amount. We did not increase the dose beyond 50  $\mu\text{mol/kg}$  of the uncleavable control because of the large quantities of peptide required (over 1  $\mu\text{mol}$  per animal) and because an uncleavable control has no diagnostic or therapeutic relevance *per se*, but serves mainly to suggest how low the systemic toxicity might ultimately be if the linker were selectively cleaved only within the tumor.

After obtaining these unexpected experimental results, the question still remained whether this toxicity of CPP and cleavable ACPP was due to rapid bolus which could be attenuated by intraperitoneal (IP) administration. Two animals were injected with 20  $\mu\text{mol/kg}$  of CPP. Initially they became slightly flushed and unresponsive for 5–10 minutes then at about 15 minutes both died as described for the iv ACPP at 10  $\mu\text{mol/kg}$ . For the cleavable ACPP, a mouse injected with a 20  $\mu\text{mol/kg}$  dose died after slow onset of clinical signs, but onset took more than an hour. Therefore IP administration does delay and attenuate the toxicity of both CPP and ACPP, likely due to slowed systemic delivery, but did not eliminate toxicity.

## Discussion

Activatable cell-penetrating peptides represent a novel strategy for targeting imaging contrast agents and therapeutic agents for cancer. This approach requires that uptake of CPPs be inhibitable by covalent linkage of a complimentary polyanionic peptide, and that such inhibition is reversible by cleavage of the linker, e.g. by proteases. Our initial publication<sup>10</sup> demonstrated the basic feasibility of ACPPs but left many questions unanswered, some of which we address here.

The idea that the polyanion blocks the polycation only as long as they are covalently tied to each other is qualitatively plausible but needs quantitative justification. Determination of the  $K_d$  for r<sub>9</sub>-e<sub>9</sub> binding confirms that this value ( $\sim 6 \mu\text{M}$ ) lies safely between the effective molarity ( $\sim 50 \text{ mM}$ ) enforced by our typical linker with 25 rotatable bonds and the probable free concentrations of each peptide attained *in vivo* ( $< 0.4 \mu\text{M}$ ). But these numbers provide some prospective guidance, not just retrospective justification. They suggest that longer linkers with as many as 50 rotatable bonds should still work, because the effective molarity would still be  $\sim 18 \text{ mM}$ .<sup>14</sup> Such extra length could be useful, either to allow substrate recognition sequences

longer than 6 amino acids, or to incorporate extra spacers to enable the peptide to adopt a more linear conformation inside the protease active site. However, major increases in the length of the polyarginine and polyglutamate repeats could well make dissociation too inefficient or too slow after linker cleavage. Major shortening of those repeats is also not advisable, because efficiency of polyarginine CPPs falls off steeply below about 8 arginines.<sup>19</sup> A naked polynucleotide chain is likely to be quite good at binding to and neutralizing polyarginine of the same number of charges, so polyarginine-mediated delivery of DNA or RNA will probably require shielding of the nucleic acid or provision of excess positive charges.

Tumors are much more brightly stained *in vivo* by ACPPs than equimolar CPPs, both imaged 6 hr after IV administration (Fig. 3C and 5B, C, D; also Fig. 3B of the accompanying paper, Olson *et al*). Thus ACPPs are considerably superior to CPPs for epifluorescence imaging, the way optical probes are normally evaluated. However, in this paper we have also introduced SUVs measured by fluorescence after homogenization of bulk tissue in SDS. Such SUVs do not yet show significantly higher tumor uptake for ACPPs over CPPs (Fig. 3D). Some of the discrepancy might be explained by the tendency of the ACPP to preferentially light up the outer edge of the tumor (Fig. 5D), which is the region most visible by macroscopic epifluorescence. Another speculative possibility is that much of the CPP is sufficiently highly concentrated, perhaps on the walls of the vasculature, that the Cy5 fluorescence undergoes self-quenching. Both forms of localization would be destroyed upon tissue homogenization.

Although our previous paper showed cells in 2-D culture with diffuse cytosolic and nuclear uptake of pre-cleaved ACPPs,<sup>10</sup> subsequent experiments in 3-D cultures and tumors *in vivo* have consistently revealed that practically all the visible fluorescence comes from perinuclear punctae, presumably endosomes. We believe the main difference from earlier studies arose from the sudden exposure of naked cells to an undepletable supply of 1.25  $\mu\text{M}$  CPP, allowing high enough accumulations in the endosomes to disrupt those organelles. In the present study, the CPP is gradually generated by *in situ* cleavage of the ACPP and is buffered by a high density of neighboring cells and extracellular matrix. Therefore endosomal concentrations may never reach the threshold required for membrane disruption though final concentration reached in tissue has been observed beyond 8–17  $\mu\text{mol/kg}$ . This reasoning suggests that the only way *in vivo* to achieve the levels of CPP currently necessary to disrupt endosomes or be taken by disruption of membrane potential (possibly in an endosome independent way)<sup>20,13</sup> would be by localized administration of high concentrations directly into a particular tissue of interest. Systemic delivery of cargoes directly linked to simple CPPs will not reach the cytoplasm or nucleus because the CPP is diluted over too many binding sites and is already toxic at modest doses. ACPPs are more tissue-specific and less toxic, but enzymatic release of the active CPP is gradual and may not be stoichiometric. Efficient *in vivo* delivery to the cytoplasm and nucleus will probably require cargoes that are either much more potently endosomolytic or that release membrane-permeant fragments. Fortunately, many applications of ACPPs, e.g. macroscopic imaging for tumor diagnosis, do not require endosomal escape.

The systemic toxicity of the free polyarginine CPP was somewhat surprising. The detailed mechanism remains to be elucidated, but toxicity is inhibited by attachment of the polyglutamate domain just as cellular uptake is. Therefore future improvements in selectivity that reduce the cleavage of the ACPP in non-tumor organs should not only increase tumor contrast but decrease systemic toxicity. The accompanying paper examines selective cleavage in greater detail.

## Experimental

### Peptide synthesis and fluorophore labeling

Peptides for imaging experiments were synthesized on an automatic peptide synthesizer (Perceptive Biosystems Pioneer or PTI Prelude) using standard protocols for fluorenylmethoxycarbonyl (Fmoc) solid-phase synthesis. They were then labeled with Cy5 using Cy5 monomaleimide or Cy5 mono NHS ester (GE Healthcare) and then purified by HPLC. Exact sequences for the CPP, the ACPP and the relatively uncleavable D-amino acid control were  $r_9$ -c(Cy5)-NH<sub>2</sub> ( $r_9$ Cy5), succinyl-e<sub>8</sub>-(x)-PLGLAG- $r_9$ -c(Cy5)-NH<sub>2</sub>, and succinyl-e<sub>8</sub>-x-plglag- $r_9$ -k(Cy5)-NH<sub>2</sub>, where d-amino acids are denoted in lower case and x denotes 6-aminohexanoyl. The peptides for toxicity experiments, purchased from Anaspec Inc. (San Jose, CA), were  $r_9$ -NH<sub>2</sub> (simple CPP), succinyl-e<sub>8</sub>-XPLGLAG- $r_9$ -NH<sub>2</sub> (MMP cleavable ACPP), and succinyl-e<sub>8</sub>-(PEG2)<sub>2</sub>- $r_9$ -NH<sub>2</sub> (uncleavable control). After purification by HPLC, their concentrations were determined by weight and confirmed by amino acid analysis (Alphalyse, Palo Alto, CA).

### Isothermal Titration Calorimetry (ITC)

All peptide solutions were in 20 mM Tris, pH 7.40, 150 mM NaCl. Peptide concentrations were determined by amino acid analysis. ITC runs were performed on a VP-ITC (Microcal LLC, Northampton, MA) instrument at 37 °C. Suc-e<sub>8</sub>-NH<sub>2</sub> (0.230 mM) in the syringe was titrated into amino- $r_9$ -NH<sub>2</sub> (0.013 mM) (these two peptides will be referred to as e<sub>9</sub> and r<sub>9</sub>). A blank run of e<sub>9</sub> into buffer alone was subtracted from the experimental data to obtain the final binding isotherm. The data were analyzed using Origin software supplied by Microcal.  $\Delta H$  and  $K_a$  values, along with their corresponding standard deviations, were determined directly by nonlinear least squares fit of the titration data, fixing n (stoichiometry of the complex) at 1.0. Ten runs were pooled to calculate the mean and standard deviation for the  $K_d$ , with a matched control (no peptide spiked into chamber) done the same day. The peptides were reversed with r<sub>9</sub> in the chamber and Suc-e<sub>8</sub> titrated in, yielding similar results.

### Enzyme cleavage assay

Recombinant MMP-1, MMP-2, MMP-3, MMP-7, MMP-8, MMP-9, MT1-MMP (MMP14), cathepsin B, thrombin, plasmin, tissue plasminogen activator (tPA), prostate specific antigen (PSA), and thrombin were obtained from EMD. Urokinase (uPA) was from Sigma and neprilysin from R&D Systems Inc. These enzymes were activated by vendors' recommended protocols if needed, then incubated at 50 nM with 3  $\mu$ M peptide for 30 minutes at 37°C. Cleavage was performed in a 20 mM Tris buffer with 150 mM NaCl and 2 mM CaCl<sub>2</sub> at pH 7.4 for all enzymes except for cathepsin B, which was tested in 50 mM sodium acetate at pH 5.0. Samples were diluted into SDS tricine loading buffer, boiled, and run on 10–20% tricine buffered polyacrylamide gels (Invitrogen). Gels were imaged to detect Cy5 labeled peptide and % peptide cleavage was determined from average signal measurements using Image J (NIH) done in triplicate.

### 3D tissue culture

HT1080 fibrosarcoma (ATCC) and MDA-MB-231 human adenocarcinoma (Bissell lab) were cultured as monolayers in Eagle's Minimal Essential Medium with 10% fetal bovine serum. For 3D culture, 1000–5000 cells were plated in 2 mg/mL Matrigel (BD biosciences) on top of a base coat in 96 well plate plates to keep cells suspended. When clusters reached 75–200  $\mu$ m diameter, they were treated for 20–24 hr with 1.5  $\mu$ M Cy5 labeled ACPP or control peptides, with or without MMP inhibitor GM6001 (EMD Biosciences), and a 1% final concentration of DMSO. Clusters were then treated with 1  $\mu$ g/mL of Calcein Green AM (Invitrogen) and 10  $\mu$ g/mL propidium iodide (EMD) to label live and dead cells respectively and subsequently

washed three times. Cell clusters were imaged at low power on a fluorescence dissecting microscope (Lumar, Zeiss) for quantification of multiple clusters, or imaged by laser scanning confocal microscopy for higher resolution (LSM5 Live, Zeiss). Average Cy5 intensity per cluster was measured from 20–40 clusters distributed over 3 images taken from duplicate treatments. Confocal images are presented as maximum projections of 50 images acquired at 1  $\mu$ m depth intervals.

### Mouse models

Pharmacokinetic distribution studies of ACPP and CPPs were performed in athymic nude mice (Charles River Labs) containing xenografts of HT1080 tumors prepared by injection of two million cells (ATCC) into the left mammary fat pad 5–7 days before peptide injection. For toxicity studies, naïve athymic nude mice were used. All procedures were approved by the UCSD Institutional Animal Care and Use Committee.

### Whole animal imaging

After tail vein injection, mice were imaged at different time points using a small animal imager (Maestro, Cambridge Research Instruments). Images were acquired with  $640 \pm 20$  nm excitation and the emission filter tuned to 700 nm (bandwidth 40nm), augmented by a 700 nm long pass filter, with exposure times between 300 ms and 1s. Blood was collected at various time points from the tail artery into capillary tubes, which were imaged for Cy5 fluorescence on the Maestro. For live animal imaging, the mice were anesthetized with 125 mg/kg of ketamine and 62.5 mg/kg of midazolam.

### Standardized Uptake Values

After euthanasia, organs were harvested, cut into 30 mg pieces, homogenized in 100 $\mu$ L 10mM Tris buffer (pH 7.6) with 1% SDS, boiled for 10 minutes, centrifuged at 20,500  $\times$  g for 10min and frozen. Tissues were then imaged while frozen on the Maestro. Integrated intensities of tissues were collected using Image J software and relative values were adjusted using a fluorescence calibration standard (USFS-336 Orange Fluorescence, Labsphere Inc.). Peptide concentration was determined from tissue fluorescence using a tissue specific standard curve (HT1080 tumor, liver, kidney and muscle from nude mice) with known amounts of  $r_9$ Cy5 peptide spiked into tissue samples and processed as above. The 3 parameter exponential rise to max ( $f=y+a*(1-\exp(-b*x))$ ; Sigmaplot) equation was used for standard curves due to nonlinearity of fluorescence at high concentrations  $> 1 \mu$ mol/kg (From these data the SUV was calculated as (moles/g tissue)/(moles injected/weight of animal)).

### Confocal imaging of live mouse tissues

Animals were injected intravenously with 250  $\mu$ g of Hoechst 33342 (Invitrogen) and 800  $\mu$ g of 2 MDa rhodamine dextran (Invitrogen) 5 min before sacrifice. Organs were then removed and kept on ice in HBSS until image. Organs were then placed on a coverslip and imaged by confocal microscopy (LSM 5 Live, Zeiss). Tissues were imaged in the order of kidney, liver, tumor, and muscle within 30 minutes of sacrifice to minimize tissue death. Images were acquired as 3D stacks with 5 – 60  $\mu$ m penetration into tissue. Cy5, Hoechst, and rhodamine were excited with 630 nm, 405 nm, and 535 nm lasers while emission was acquired with 650 nm LP, 420 nm LP, and 550 nm LP filters respectively.

### Toxicity of CPP and ACPPs in mice

Peptides dissolved in 50  $\mu$ l of water were injected into the tail vein under isoflurane anesthesia. For ip injection of peptide mice were not anesthetized. Immediately after injection, isoflurane was removed and mice were allowed to wake up under observation. Body masses were measured before and 24 hours after injection (if the animal survived injection) to detect

significant weight loss due to toxicity. Toxicity was assayed both qualitatively and quantitatively by clinical observation of healthy vs moribund behavior, and death.

## Supplementary Material

Refer to Web version on PubMed Central for supplementary material.

## Acknowledgments

We thank Mina Bissell for instruction on 3-D cultures and cells; Perla Acaria for processing of SUV tissues; Mike Whitney for assistance in peptide synthesis and discussion; Jessica Crisp for expertise and assistance performing enzyme cleavage assay and important discussion; Qing Xing for assistance in peptide synthesis; this work was supported by grant W81XWH-05-1-0183 from the Dept. of Defense Breast Cancer Research Program.

## Abbreviations

|      |                                       |
|------|---------------------------------------|
| CPP  | cell penetrating peptides             |
| ACPP | activatable cell penetrating peptides |
| MMP- | matrix metalloproteinase              |
| SUV  | standardized uptake value             |

## Reference List

1. Torchilin VP. Tat peptide-mediated intracellular delivery of pharmaceutical nanocarriers. *Adv. Drug Deliv. Rev* 2008;60:548–558. [PubMed: 18053612]
2. Patel LN, Zaro JL, Shen WC. Cell penetrating peptides: intracellular pathways and pharmaceutical perspectives. *Pharm. Res* 2007;24:1977–1992. [PubMed: 17443399]
3. Lundberg M, Johansson M. Is VP22 nuclear homing an artifact? *Nat. Biotechnol* 2001;19:713–714. [PubMed: 11479552]
4. Richard JP, Melikov K, Vives E, Ramos C, Verbeure B, Gait MJ, Chernomordik LV, Lebleu B. Cell-penetrating peptides. A reevaluation of the mechanism of cellular uptake. *J. Biol. Chem* 2003;278:585–590. [PubMed: 12411431]
5. Schwarze SR, Ho A, Vocero-Akbani A, Dowdy SF. In vivo protein transduction: delivery of a biologically active protein into the mouse. *Science* 1999;285:1569–1572. [PubMed: 10477521]
6. Snyder EL, Meade BR, Dowdy SF. Anti-cancer protein transduction strategies: reconstitution of p27 tumor suppressor function. *J. Control Release* 2003;91:45–51. [PubMed: 12932636]
7. Mai JC, Mi Z, Kim SH, Ng B, Robbins PD. A proapoptotic peptide for the treatment of solid tumors. *Cancer Res* 2001;61:7709–7712. [PubMed: 11691780]
8. Snyder EL, Meade BR, Saenz CC, Dowdy SF. Treatment of terminal peritoneal carcinomatosis by a transducible p53-activating peptide. *PLoS. Biol* 2004;2:E36. [PubMed: 14966535]
9. Dubikovskaya EA, Thorne SH, Pillow TH, Contag CH, Wender PA. Overcoming multidrug resistance of small-molecule therapeutics through conjugation with releasable octaarginine transporters. *Proc. Natl. Acad. Sci. U. S. A* 2008;105:12128–12133. [PubMed: 18713866]
10. Jiang T, Olson ES, Nguyen QT, Roy M, Jennings PA, Tsien RY. Tumor imaging by means of proteolytic activation of cell-penetrating peptides. *Proc. Natl. Acad. Sci. U. S. A* 2004;101:17867–17872. [PubMed: 15601762]
11. Polyakov V, Sharma V, Dahlheimer JL, Pica CM, Luker GD, Piwnica-Worms D. Novel Tat-peptide chelates for direct transduction of technetium-99m and rhenium into human cells for imaging and radiotherapy. *Bioconjug. Chem* 2000;11:762–771. [PubMed: 11087323]
12. Lee HJ, Partridge WM. Pharmacokinetics and delivery of tat and tat-protein conjugates to tissues in vivo. *Bioconjug. Chem* 2001;12:995–999. [PubMed: 11716691]

13. Kosuge M, Takeuchi T, Nakase I, Jones AT, Futaki S. Cellular internalization and distribution of arginine-rich peptides as a function of extracellular peptide concentration, serum, and plasma membrane associated proteoglycans. *Bioconjug. Chem* 2008;19:656–664. [PubMed: 18269225]
14. Galli C, Mandolini L. The role of ring strain on the ease of ring closure of bifunctional chain molecules. *Eur. J. Org. Chem* 2000;2000:3117–3125.
15. Kasper G, Reule M, Tschirschmann M, Dankert N, Stout-Weider K, Lauster R, Schrock E, Mennerich D, Duda GN, Lehmann KE. Stromelysin-3 over-expression enhances tumourigenesis in MCF-7 and MDA-MB-231 breast cancer cell lines: involvement of the IGF-1 signalling pathway. *BMC. Cancer* 2007;7:12. [PubMed: 17233884]
16. Vives E. Present and future of cell-penetrating peptide mediated delivery systems: "is the Trojan horse too wild to go only to Troy?". *J. Control Release* 2005;109:77–85. [PubMed: 16271792]
17. Wadia JS, Dowdy SF. Transmembrane delivery of protein and peptide drugs by TAT-mediated transduction in the treatment of cancer. *Adv. Drug Deliv. Rev* 2005;57:579–596. [PubMed: 15722165]
18. Albright CF, Graciani N, Han W, Yue E, Stein R, Lai Z, Diamond M, Dowling R, Grimminger L, Zhang SY, Behrens D, Musselman A, Bruckner R, Zhang M, Jiang X, Hu D, Higley A, Dimeo S, Rafalski M, Mandlekar S, Car B, Yeleswaram S, Stern A, Copeland RA, Combs A, Seitz SP, Trainor GL, Taub R, Huang P, Oliff A. Matrix metalloproteinase-activated doxorubicin prodrugs inhibit HT1080 xenograft growth better than doxorubicin with less toxicity. *Mol. Cancer Ther* 2005;4:751–760. [PubMed: 15897239]
19. Wender PA, Mitchell DJ, Pattabiraman K, Pelkey ET, Steinman L, Rothbard JB. The design, synthesis, and evaluation of molecules that enable or enhance cellular uptake: peptoid molecular transporters. *Proc. Natl. Acad. Sci. U. S. A* 2000;97:13003–13008. [PubMed: 11087855]
20. Rothbard JB, Jessop TC, Lewis RS, Murray BA, Wender PA. Role of membrane potential and hydrogen bonding in the mechanism of translocation of guanidinium-rich peptides into cells. *J. Am. Chem. Soc* 2004;126:9506–9507. [PubMed: 15291531]

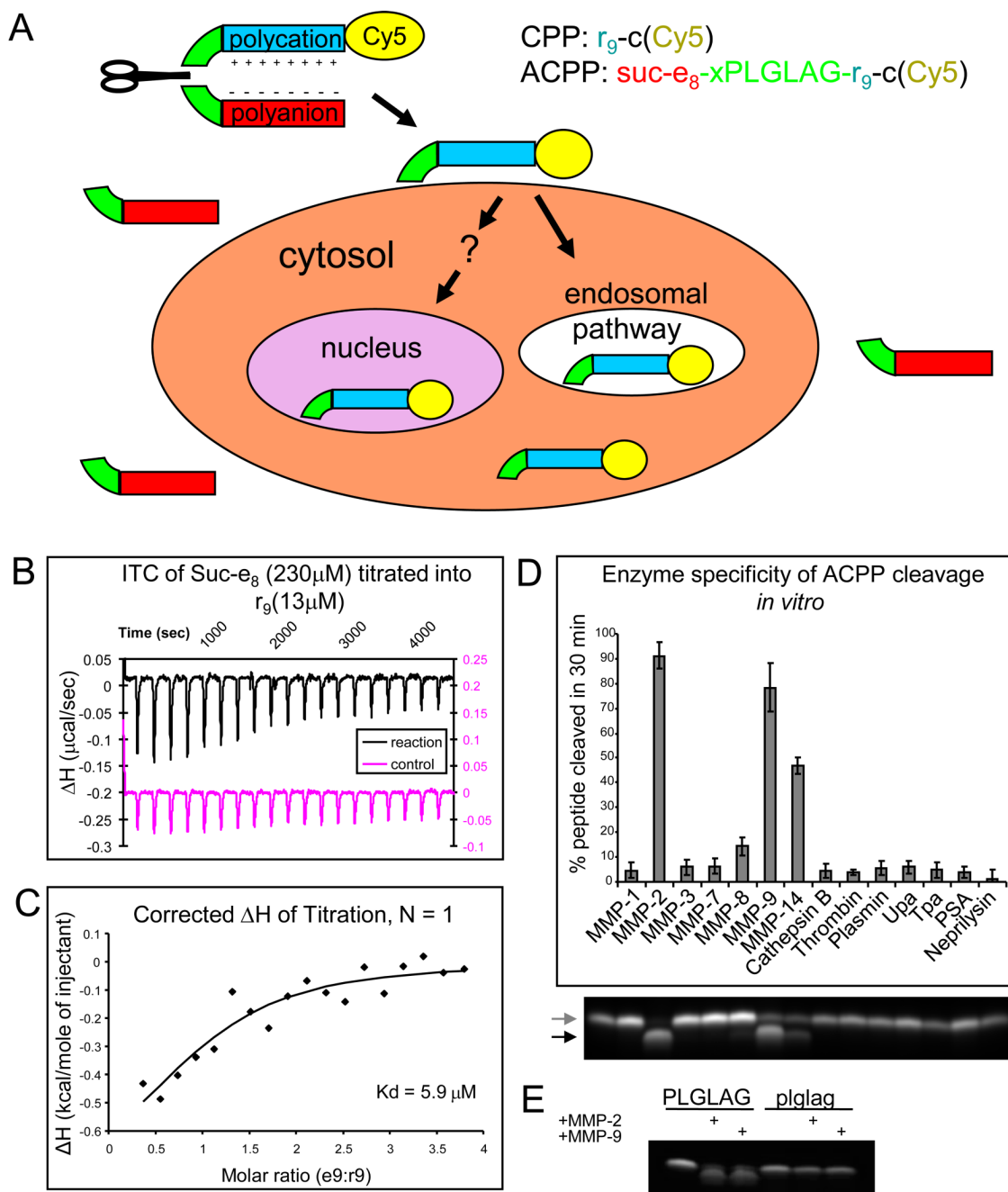


**Fig. 1.** ACPPs selectively unmask CPPs upon protease cleavage of a linker, which is selective for MMPs when the linker sequence is PLGLAG. (A) General scheme for ACPPs. While the linker (green) between the polyanion (red) and polycation (blue) sequences remains intact, cell uptake is blocked and the entire molecule can enter the extracellular space of tissues and wash out. Once a protease (symbolized by a scissor) cuts the linker, the polyglutamate dissociates, allowing the polyarginine and its payload (yellow, in current examples Cy5) to immediately adhere to cells and eventually become endocytosed. (B) Isothermal titration calorimetry raw data showing the change in enthalpy as 230  $\mu$ M Suc- $e_8$  is titrated into a 13  $\mu$ M solution of  $r_9$ . (C) These raw data can be corrected for and the change in enthalpy can be plotted as a function

of molar ratio of the two peptides yielding determination of the  $K_d$ . (D) The percentage by which the polycation is released as a result of cleaving the PLGLAG linker after 30 minute incubation with 50 nM protease. Cleavage of the peptide was detected by tricine SDS-PAGE, a representative fluorescence image of a gel is shown below with first lane being uncleaved peptide. The following lanes line up with the chart above. Arrows point to uncleaved peptide (upper grey arrow) and cleaved peptide (lower black arrow). (E) D-amino acid control Suc-e<sub>8</sub>-xplglag-r<sub>9</sub>-c(Cy5) remains uncut by MMP-2 and MMP-9 under conditions where the ACPP Suc-e<sub>8</sub>-xPLGLAG-r<sub>9</sub>-c(Cy5) is cleaved.

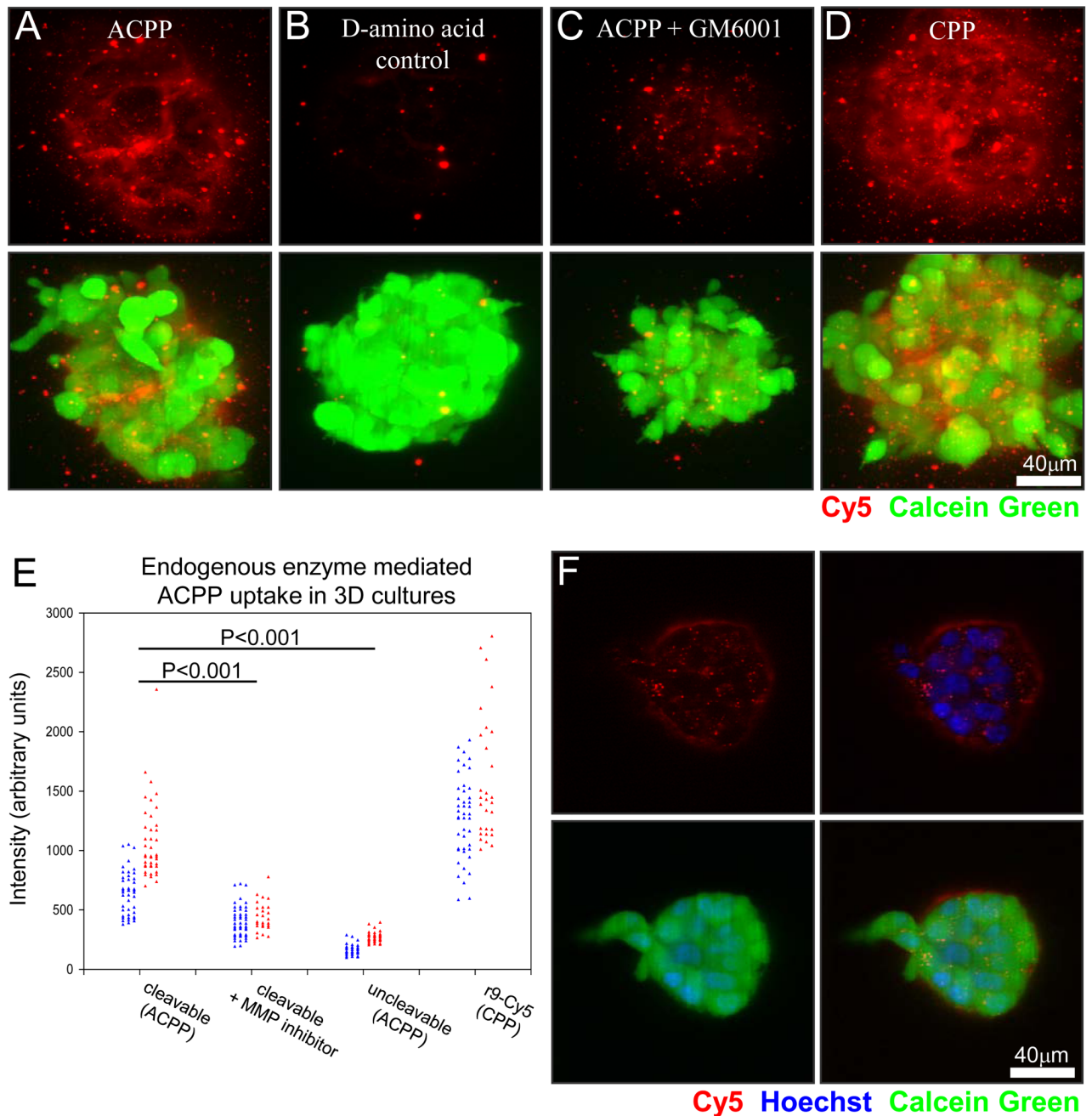


**Fig. 2.** MMP cleavable PLGLAG linker built into the ACPP shows uptake due to endogenous proteases in a 3-D tissue culture model. (A, B) MDA-MB-231 cluster confocal maximum projections of cleavable PLGLAG ACPP versus uncleavable d-amino acid peptide (red) show micro localization of peptide and differential uptake due to the presence of the cleavable linker. (C) Shows decreased cleavable ACPP peptide when co-incubated with 100  $\mu$ M broad spectrum MMP inhibitor GM6001. (D) r<sub>9</sub>Cy5 CPP positive control shows uptake of CPP throughout 3-D clusters. Scale bar for A–D is 40  $\mu$ m. (E) Comparison of the average intensity of multiple 3-D clusters of HT1080 fibrosarcoma (red) or MDA-MB-231 mammary adenocarcinoma (blue) cells treated with PLGLAG cleavable ACPP, ACPP + GM6001 MMP inhibitor,

uncleavable d-amino acid ACPP, and r<sub>9</sub>Cy5 CPP control (t-test p-value for significance labeled accordingly). Cell clusters were incubated with 1.5 μM peptide for 24hrs then washed (3x), counterstained with calcein green AM ester (cell viability, green), and then imaged. (F) Representative confocal slice of a 3-D cluster showing ACPP uptake into subcellular puncta, cell surface, and extracellular matrix of live cells. ACPP is shown in red, Hoechst 33342 counter stain for cell nuclei (blue), and calcein green AM (green) to show live cells.

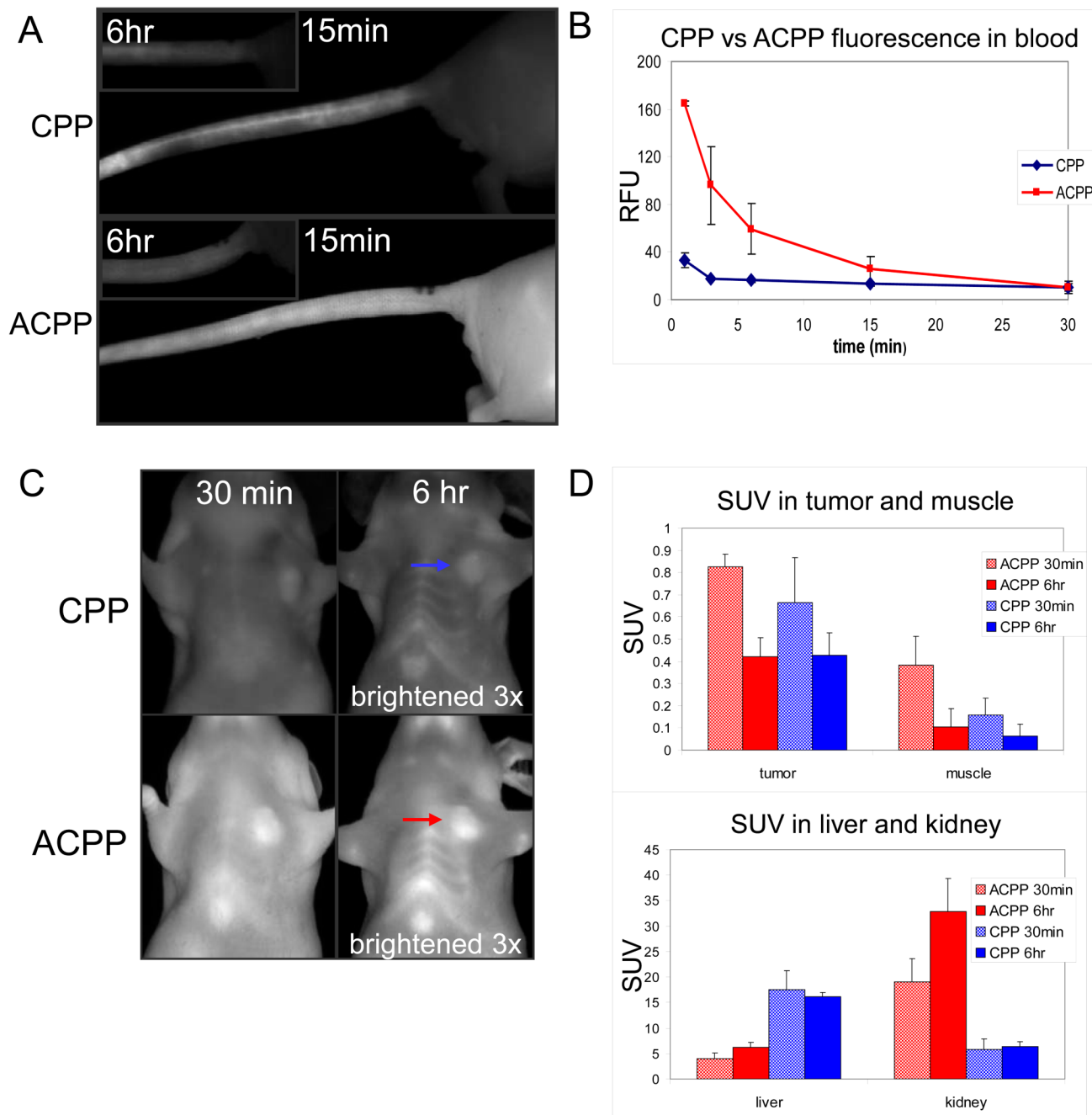


**Fig. 3.** Comparison of pharmacokinetic tissue distribution between CPP and ACPP following intravenous injection into HT-1080 tumor bearing nude mice reveals differences in peptide distribution. (A) Images showing tail veins of animals injected with CPP (top) and ACPP (bottom) at the indicated time points following injection. (B) Cy5 fluorescence in the blood throughout the first 30 minutes after injection as an average of three mice for CPP and ACPP. Tumors are indicated by arrows. (C) Representative HT-1080 mice injected with CPP and ACPP were imaged at 30 minutes and 6 hours (6 hour images brightened 3x). (D) Standardized uptake value (SUV, moles/g in tissue / moles injected/weight of animal) of peptide in tumor, muscle, liver, and kidney, showing changes over time between ACPP and CPP injection. (n=4

for all 6 hour mice, n=5 for all organs of 30 minute mice, n=4 and n=3 for ACPP and CPP tumors of 30 minute mice).

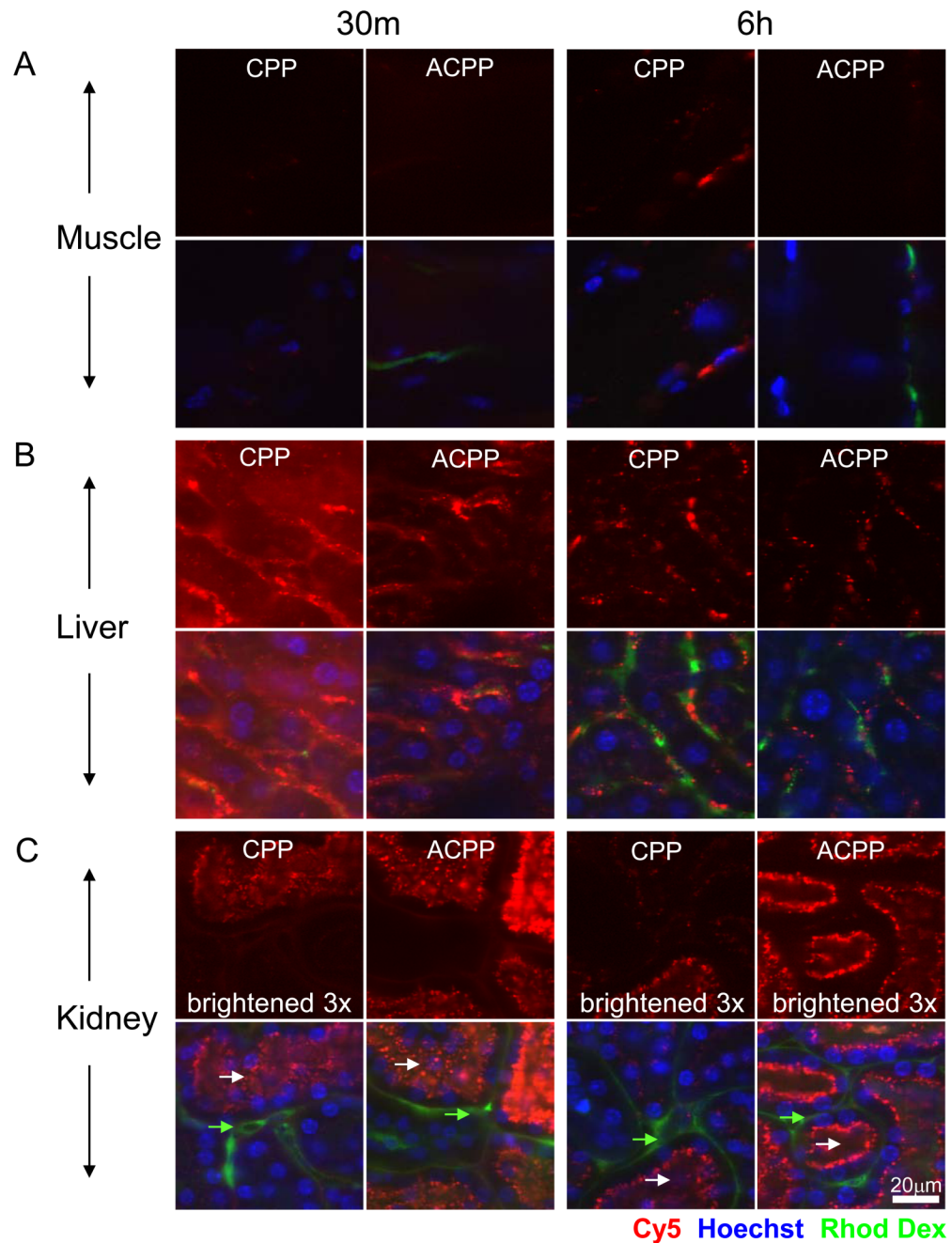


**Fig. 4.** Confocal microscopy of CPP and ACPP in organs revealed peptide localization to endosomes in nude mice. The figure shows confocal slices of Cy5 peptide (red) and then overlay with nuclei (Hoechst 33342- blue) and blood pool (rhodamine dextran -green). Images are of muscle (A), liver (B), and kidney (C) at 30 minutes and 6 hours after IV injection of 10 nmol of peptide as specified. No significant nuclear uptake was observed in any tissue for either the CPP or the ACPP. Peptide signal was scaled equally for each organ to visualize subcellular distribution and a difference in scaling in a particular tissue is labeled accordingly. White arrows point to lumen of renal tubules and green arrows point to basal lateral/blood flow region of renal tubules. Scale bar is 20 μm.

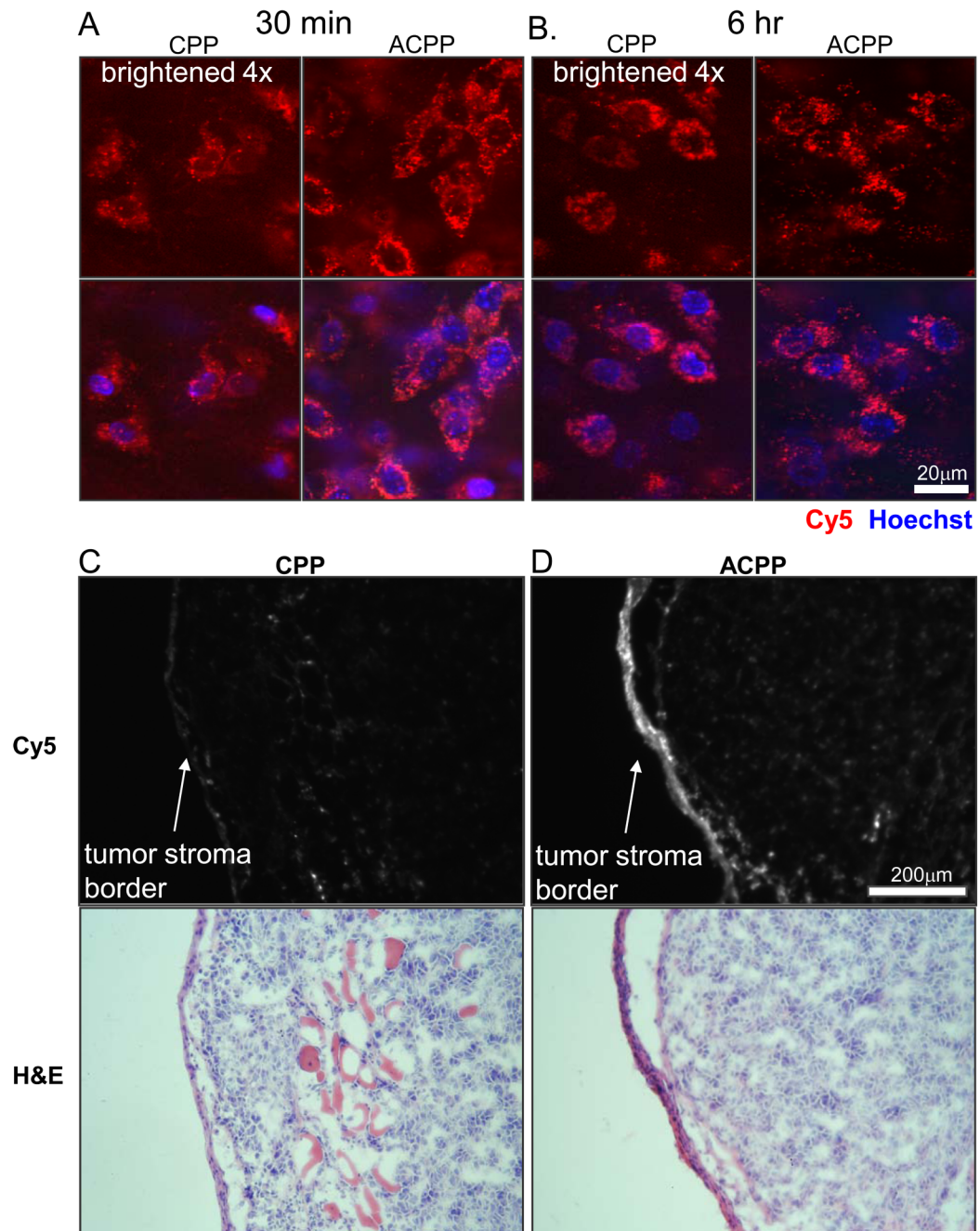


**Fig. 5.** Confocal microscopy reveals no significant nuclear uptake of ACPP or CPP in HT1080 xenografts. Confocal slice of HT1080 tumors from mice injected with CPP and ACPP at 30 minutes (A) and 6 hours (B). Mice were injected with Cy5 peptide (red) at 30 minutes or 6 hours before imaging and Hoechst 33342 nuclear stain (blue) 5 min before imaging to demonstrate that ACPP uptake is in cytoplasmic perinuclear structures but not in nuclei. Upper image is Cy5 peptide alone and lower image shows overlay with Hoechst. The CPP images were scaled brighter by a factor of 4 to visualize intracellular peptide containing punctae. Scale bar is 20 μm. (C, D) Show Cy5 fluorescence of frozen sections from mice 6 hours after injection

of CPP or ACPP, highlighting greater uptake with ACPP particularly at leading stromal edge of tumors. Scale bar 200  $\mu$ M.

**Table 1**

Summary of CPP and ACPD acute toxicity in mice. Nude mice were IV injected with peptide and observed for acute toxicity resulting in rapid death. Mouse survival of immediate period after injection was recorded, each showing no signs of moribundity or significant weight loss for at least 2 days post injection. Unlabeled peptide injected, dose injected IV, range of mice mass, time of death, and number survived (minimal 24 hours with no signs of toxicity) are listed in the table.

| Peptide                             | Dose                           | Mouse Mass (range) | Time of death    | Survived |
|-------------------------------------|--------------------------------|--------------------|------------------|----------|
| r <sub>9</sub> CPP                  | 2.5 μmol/kg (53–65 nmols)      | 21.7–26.0g         | 15–20 min<br>n=1 | 4/5      |
|                                     | 5 μmol/kg (105–117 nmols)      | 21.0–25.7g         | <3 min<br>n=5    | 0/5      |
| PLGLAG cleavable ACPD               | 10 μmol/kg (220–266 nmols)     | 22.3–26.6g         | NA               | 5/5      |
|                                     | 20 μmol/kg (352–480 nmols)     | 16.0–24.0g         | 10–20 min<br>n=5 | 0/5      |
| (PEG) <sub>2</sub> uncleavable ACPD | 10 μmol/kg (182, 202 nmols)    | 20.6–23.3g         | NA               | 2/2      |
|                                     | 20 μmol/kg (405 nmols)         | 20.2–21.2g         | NA               | 2/2      |
|                                     | 50 μmol/kg (1,100–1,280 nmols) | 22.0–25.6g         | NA               | 3/3      |